*Inorg. Chem.* **2008**, *47*, 8972−8984

# Transformation of Proton-Conducting Perovskite-Type into Fluorite-Type Fast Oxide Ion Electrolytes Using a $CO_2$ Capture Technique and Their Electrical Properties

**Francesca Trobec and Venkataraman Thangadurai***

*Department of Chemistry, University of Calgary, 2500 University Drive NW, Calgary, Alberta, T2N 1N4 Canada*

Received May 31, 2008

Fast oxide ion conducting $Ce_{1-x}M_xO_{2-\delta}$ (M = In, Sm; $x = 0.1$, 0.2) and $Ce_{0.8}Sm_{0.05}Ca_{0.15}O_{1.825}$ were prepared from the corresponding perovskite-like structured materials with nominal chemical composition of $BaCe_{1-x}M_xO_{3-\delta}$ and $BaCe_{0.8}Sm_{0.05}Ca_{0.15}O_{2.825}$, respectively, by reacting with $CO_2$ at 800 °C for 12 h. Powder X-ray diffraction (PXRD) analysis showed the formation of fluorite-type $CeO_2$ and $BaCO_3$ just after reaction with $CO_2$. The amount of $CO_2$ gained per ceramic gram was found to be consistent with the Ba content. The $CO_2$ reacted samples were washed with dilute HCl and water, and the resultant solid product was characterized structurally and electrically employing various solid-state characterization methods, including PXRD, and alternating current (ac) impedance spectroscopy. The lattice constant of presently prepared $Ce_{1-x}M_xO_{2-\delta}$ and $Ce_{0.8}Sm_{0.05}Ca_{0.15}O_{1.825}$ by a $CO_2$ capture technique follows the expected ionic radii trend. For example, In-doped $Ce_{0.9}In_{0.1}O_{1.95}$ ($In^{3+}_{(VIII)} = 0.92$ Å) sample showed a fluorite-type cell constant of 5.398(1) Å, which is lower than the parent $CeO_2$ (5.411 Å, $Ce^{4+}_{(VIII)} = 0.97$ Å). Our attempt to prepare single-phase In-doped $CeO_2$ samples at 800, 1000, and 1500 °C using the ceramic method was unsuccessful. However, we were able to prepare single-phase $Ce_{0.9}In_{0.1}O_{1.95}$ and $Ce_{0.8}In_{0.2}O_{1.9}$ by the $CO_2$ capture method from the corresponding barium perovskites. The PXRD studies showed that the In-doped samples are thermodynamically unstable above 800 °C. The ac electrical conductivity studies using Pt electrodes showed the presence of bulk, grain-boundary, and electrode contributions over the investigated temperature range in the frequency range of $10^{-2}$−$10^7$ Hz. The bulk ionic conductivity and activation energy for the electrical conductivity of presently prepared Sm- and (Sm + Ca)-doped $CeO_2$ samples shows conductivities similar to those of materials prepared by the ceramic method reported in the literature. For instance, the conductivity of $Ce_{0.8}Sm_{0.2}O_{1.9}$ using the $CO_2$ capture technique was determined to be $4.1 \times 10^{-3}$ S/cm, and the conductivity of the same sample prepared using the ceramic method was $3.9 \times 10^{-3}$ S/cm at 500 °C. The apparent activation energy of the area-specific polarization resistance for the symmetric cell $(Sm,Sr)CoO_{3-x}|Ce_{0.8}Sm_{0.2}O_{1.9}|(Sm,Sr)CoO_{3-x}$ was determined to be 1 eV in air.

## 1. Introduction

Recently, conversion of chemical reaction energy into electrical energy has been considered as a modern energy source because of its potential for present energy needs as well as future stationary, portable, and transport applications.[1−5] In this regard, fuel cells, especially solid oxide fuel cells (SOFCs), have drawn much attention because of their modular and distributed nature, zero noise pollution, and low levels of emissions, greenhouse gases, and toxic gases.[4] SOFCs can be operated over a wide range of temperatures (500−1000 °C). Furthermore, such high-operational-temperature SOFCs offer significant advantages over conventional low-temperature polymer-based proton-exchange mem-

* To whom correspondence should be addressed. E-mail: vthangad@ucalgary.ca.

(1) Ormerod, R. M. *Chem. Soc. Rev.* **2003**, *32*, 17–28.
(2) Stambouli, A. B.; Traversa, E. *Renewable Sustainable Energy Rev.* **2002**, *6*, 433–455.
(3) Steele, B. C. H.; Heinzel, A. *Nature* **2001**, *414*, 345–352.
(4) Carrette, L.; Friedrich, K. A.; Stimming, U. *Fuel Cells* **2001**, *1*, 5–39.
(5) Kreuer, K. D. *Chem. Mater.* **1996**, *8*, 610–641.



10.1021/ic8010025 CCC: $40.75 
Published on Web 08/16/2008

brane fuel cells, as well as molten salt or liquid-based fuel cells.[6−10] These advantages include direct utilization of dirty hydrocarbon fuels,[1,2] high efficiency (about 90% including heat recovery),[2] the use of cheap ceramic oxides as electrodes, and the use of established economic ceramic processing technology.

In the current SOFC, the electrolyte conducts predominately oxide ions ($O^{2-}$) and is electronically insulating between the employed oxygen activities from the air to fuel side.[11] The electrodes must be porous, mixed ionic−electronic conductors, allowing electrons to travel through an external circuit. Current commercialization of SOFCs appears to be based primarily on the fluorite-type $Y_2O_3$-doped $ZrO_2$ (YSZ) electrolyte, a Ni-YSZ cermet anode, the perovskite-type Sr-doped $LaMnO_3$ cathode, and a Ca- or Sr-doped $LaCrO_3$ interconnect.[6−8,12−17] SOFCs based on YSZ require high operating temperatures (750−1000 °C) because YSZ exhibits much lower ionic conduction at low temperatures. Such a high operational temperature has been considered as a potential materials problem in the development of long-term stable SOFCs because of detrimental mechanical stress induced between electrolytes and electrodes, the formation of interfacial reaction products due to diffusion of strontium and lanthanum from the cathode to the electrolyte, a lack of long-term chemically stable sealing materials, and the large cost of bipolar separators.[17−20] Attempts have been made to replace conventional YSZ electrolytes in SOFCs by other intermediate-temperature (IT) oxide ion electrolytes.[8,12,21−25] It must be mentioned that both Sr- and Mg-doped perovskite-like $LaGaO_3$ (LSGM),[26−28] and Sm- or Gd-doped $CeO_2$ are presently accepted as the most promising candidate electrolytes for the development of IT-SOFCs.[21,29−39]

Among the IT-SOFC electrolytes, fluorite-type structured $Ce_{1-x}M_xO_{2-\delta}$ (M = Sm, Gd) have drawn much attention because of their high oxide ion conductivity compared to YSZ and LSGM.[40] Also, $CeO_2$-based electrolytes show better chemical stability against reaction with anode Ni as well as several perovskite-type structure cathode materials, including $La_{1-x}Sr_xMnO_3$ (LSM), $La_{0.5}Sr_{0.5}CoO_{3-\delta}$ (LSC), $La_{1-x}Sr_xFeO_3$ (LSF), $La_{1-x}Sr_xCo_{1-y}Fe_yO_3$ (LSCF), and $LaNa_{1-x}Fe_xO_3$ (LNF) cathodes.[41−44] Several studies were performed to understand the effect of synthesis methods and microstructure on the electrical conductivity of $CeO_2$ and to decrease the large grain-boundary (a common problem with doped $CeO_2$ electrolyte) resistance to the total conductivity.[45−54] The employed preparation methods include polymerization, sol−gel, and precipitation. Recently, we have prepared Y-doped $CeO_2$ from Y-doped $BaCeO_3$ by making use of the $CO_2$ reaction.[55] In the present work, we have extended this idea to prepare the most promising fast oxide ion conducting In- or Sm-doped $CeO_2$ and $Ce_{0.8}Sm_{0.05}Ca_{0.15}O_{1.825}$ using the perovskite-like $BaCe_{1-x}M_xO_{3-\delta}$ (M = In, Sm) and $BaCe_{0.8}Sm_{0.05}Ca_{0.15}O_{2.825}$ as precursors, respectively. Interestingly, we were able to stabilize In-doped $CeO_2$ materials at 800 °C. To our knowledge, this is the first instance in which the single-phase In-containing fluorite material has been prepared and characterized.


(6) Lashtabeg, A.; Skinner, S. J. *J. Mater. Chem.* **2006**, *16*, 3161–3170.
(7) Singh, P.; Minh, N. Q. *Int. J. Appl. Ceram. Technol.* **2004**, *1*, 5–15.
(8) Haile, S. M. *Acta Mater.* **2003**, *51*, 5981–6000.
(9) Dokiya, M. *Solid State Ionics* **2002**, *152−153*, 383–392.
(10) Minh, N. Q. *J. Am. Ceram. Soc.* **1993**, *76*, 563–588.
(11) Yamamoto, O. *Electrochim. Acta* **2000**, *45*, 2423–2435.
(12) Fergus, J. *J. Power Sources* **2006**, *162*, 30–40.
(13) Jiang, S. P.; Chan, S. H. *J. Mater. Sci.* **2004**, *39*, 4405–4439.
(14) Leng, Y. J.; Chan, S. H.; Khor, K. A.; Jiang, S. P. *J. Appl. Electrochem.* **2004**, *34*, 409–415.
(15) Brandon, N. P.; Skinner, S.; Steele, B. C. H. *Annu. Rev. Mater. Res.* **2003**, *33*, 183–213.
(16) Tietz, F.; Buchkremer, H.-P.; Stover, D. *Solid State Ionics* **2002**, *152−153*, 373–381.
(17) Steele, B. C. H. *Solid State Ionics* **1996**, *86−88*, 1223–1234.
(18) Yokokawa, Y. *Annu. Rev. Mater. Res.* **2003**, *33*, 581–610.
(19) Yokokawa, H.; Sakai, N.; Kawada, T.; Dokiya, M. *J. Electrochem. Soc.* **1991**, *138*, 2719–2727.
(20) Jorgensen, M. J.; Primdahl, S.; Mogensen, M. *Electrochim. Acta* **1999**, *44*, 4195–4201.
(21) Kharton, V. V.; Marques, F. M. B.; Atkinson, A. *Solid State Ionics* **2004**, *174*, 135–149.
(22) Weber, A.; Tiffee, E. I. *J. Power Sources* **2004**, *127*, 273–283.
(23) Boivin, J. C.; Mairesse, G. *Chem. Mater.* **1998**, *10*, 2870–2888.
(24) Kendall, K. R.; Navas, C.; Thomas, J. K.; Loye, H. *Chem. Mater.* **1996**, *8*, 642–649.
(25) Etsell, T. H.; Flengas, S. N. *Chem. Rev.* **1970**, *70*, 339–376.
(26) Ishihara, T.; Matsuda, H.; Takita, Y. *J. Am. Chem. Soc.* **1994**, *116*, 3801–3803.
(27) Huang, P.; Petric, A. *J. Electrochem. Soc.* **1996**, *143*, 1644–1648.
(28) Huang, K.; Tichy, R. S.; Goodenough, J. B. *J. Am. Ceram. Soc.* **1998**, *81*, 2565–2575.
(29) Fu, Y.; Wen, S.; Lu, C. *J. Am. Ceram. Soc.* **2008**, *91*, 127–131.
(30) Zhan, Z.; Barnett, S. A. *Science* **2005**, *308*, 844–847.
(31) Huang, W.; Wan, J.; Goodenough, J. B. *J. Mater. Sci.* **2001**, *36*, 1093–1098.
(32) Steele, B. C. H. *Solid State Ionics* **2000**, *129*, 95–110.
(33) Hibino, T.; Hashimoto, A.; Inoue, T.; Tokuno, J.; Yoshida, S.; Sano, M. *Science* **2000**, *288*, 2031–2033.
(34) Mogensen, M.; Sammes, N. M.; Tompsett, G. A. *Solid State Ionics* **2000**, *129*, 63–94.
(35) Godickemeier, M.; Gauckler, L. J. *J. Electrochem. Soc.* **1998**, *145*, 414–421.
(36) Eguchi, K. *J. Alloys Compd.* **1997**, *250*, 486–491.
(37) (a) Subbarao, E. C.; Maiti, H. S. *Solid State Ionics* **1984**, *11*, 317–338. (b) Inaba, H.; Tagawa, H. *Solid State Ionics* **1996**, *83*, 1–16.
(38) Eguchi, K.; Setoguchi, T.; Inoue, T.; Arai, H. *Solid State Ionics* **1992**, *52*, 165–172.
(39) Yahiro, H.; Eguchi, Y.; Eguchi, K.; Arai, H. *J. Appl. Electrochem.* **1988**, *18*, 527–531.
(40) Goodenough, J. B. *Annu. Rev. Mater. Res.* **2003**, *33*, 91–128.
(41) Corbel, G.; Mestiri, S.; Lacorre, P. *Solid State Sci.* **2005**, *7*, 1216–1224.
(42) Adler, S. B. *Chem. Rev.* **2004**, *104*, 4791–4843.
(43) Hart, N. T.; Brandon, N. P.; Day, M. J.; Lapena-Rey, N. *J. Power Sources* **2002**, *106*, 42–50.
(44) Tsai, T.; Barnett, S. A. *Solid State Ionics* **1997**, *98*, 191–196.
(45) Gil, V.; Moure, C.; Duran, P.; Tartaj, J. *Solid State Ionics* **2007**, *178*, 359–365.
(46) Jadhav, L. D.; Pawar, S. H.; Chourashiya, M. G. *Bull. Mater. Sci.* **2007**, *30*, 97–100.
(47) Tian, C.; Chan, S. W. *Solid State Ionics* **2000**, *134*, 89–102.
(48) Hatchwell, C.; Sammes, N. M.; Brown, I. W. M. *Solid State Ionics* **1999**, *126*, 201–208.
(49) Shemilt, J. E.; Williams, H. M. *J. Mater. Sci. Lett.* **1999**, *18*, 1723–1737.
(50) Hong, S. J.; Mehta, K.; Virkar, A. V. *J. Electrochem. Soc.* **1998**, *145*, 638–647.
(51) Torrens, R. S.; Sammes, N. M.; Tompsett, G. A. *Solid State Ionics* **1998**, *111*, 9–15.
(52) Huang, K.; Feng, M.; Goodenough, J. B. *J. Am. Ceram. Soc.* **1998**, *81* (2), 357–362.
(53) Huang, W.; Greenblatt, M. *Solid State Ionics* **1997**, *100*, 23–27.
(54) Huang, W.; Greenblatt, M. *Chem. Mater.* **1997**, *9*, 2240–2245.
(55) Sneha, B. R.; Thangadurai, V. *J. Solid State Chem.* **2007**, *180*, 2661–2669.

**Table 1.** Lattice Parameters of Parent Perovksite-Like Compounds and Their $CO_2$ Capturing Values at 800 °C

| compound | lattice parameter (Å) | | | theoretical $CO_2$ capture per ceramic gram | experimental $CO_2$ capture per ceramic gram | percent capture (%) |
|---|---|---|---|---|---|---|
| | *a* | *b* | *c* | | | |
| $BaCe_{0.9}Sm_{0.1}O_{2.95}$ | 4.3897(7) | 4.3897(7) | 4.3897(7) | 0.1351 | 0.1334 | 98.7 |
| $BaCe_{0.8}Sm_{0.2}O_{2.9}$ | 4.3900(8) | 4.3900(8) | 4.3900(8) | 0.1350 | 0.1327 | 98.3 |
| $BaCe_{0.8}Sm_{0.05}Ca_{0.15}O_{2.825}$ | 8.768(9) | 6.869(5) | 5.750(1) | 0.1428[a] | 0.1423 | 99.6 |
| | | | | 0.1642[b] | 0.1423 | 99.6 |
| $BaCe_{0.9}In_{0.1}O_{2.95}$ | 8.729(1) | 8.729(1) | 8.729(1) | 0.1366 | 0.1357 | 99.3 |
| $BaCe_{0.8}In_{0.2}O_{2.9}$ | 8.716(1) | 8.716(1) | 8.716(1) | 0.1381 | 0.1371 | 99.3 |
| CaO[c] | | | | 0.7848 | 0.7324 | 93.0 |
| $Sm_2O_3$ (99.9%, Alfa Aesar) | | | | | negligible | |
| $In_2O_3$ (99.9%, Alfa Aesar) | | | | | negligible | |

[a] Due to the Ba contribution; [b] Due to both Ba and Ca contributions. [c] Prepared from calcination of $CaCO_3$ (99%, Fisher Scientific) at 1000 °C for 24 h.

## 2. Experimental Aspects

**2.1. Preparation of Perovskite-Type Precursors.** Materials with nominal chemical formulas of $BaCe_{0.9}Sm_{0.1}O_{2.95}$, $BaCe_{0.8}Sm_{0.2}O_{2.9}$, $BaCe_{0.8}Sm_{0.05}Ca_{0.15}O_{2.825}$, $BaCe_{0.9}In_{0.1}O_{2.95}$, and $BaCe_{0.8}In_{0.2}O_{2.9}$ were prepared by employing a ceramic reaction in air using appropriate amounts of high-purity $BaCO_3$ (99+%, VWR International), $CeO_2$ (99.5%, Alfa Aesar), $Sm_2O_3$ (99.9%, Alfa Aesar), $CaCO_3$ (99%, Fisher Scientific), and $In_2O_3$ (99.9%, Alfa Aesar). $Sm_2O_3$ was predried in air for at least 2 days at 850 °C before use. The powders were mixed using a ball mill (Pulverisette, Fritsch, Germany) for 6 h at 200 rpm using zirconia balls and 2-propanol with an intermediate change in the rotation direction every 1 h to ensure proper mixing. The powders were then dried and heated in air at 1000 °C for 12 h in a clean alumina crucible. The resulting mixture was ball-milled using 2-propanol again for about 6 h and then pressed into pellets (~1 cm diameter and ~2 cm length) using an isostatic pressure of about 8 MPa. The pressed green pellets were sintered in air at 1400 °C for 24 h for the Sm samples and 1500 °C for 24 h for the In samples. The pellets were then ball-milled into a powder for powder X-ray diffraction (PXRD) characterization using a Bruker D8 powder X-ray diffractometer (Cu K$\alpha$) at room temperature with a $2\theta$ step scan width of 0.02° and a counting time of 6 s. The lattice constant was determined from the PXRD data by least-squares refinement.

**2.2. Conversion of Perovskites into Fluorite-Type Phases.** A desired known amount (typically 15−25 g) of the barium perovskite compounds was reacted with pure $CO_2$ at 800 °C for 12 h. The powder was cooled to room temperature under a $CO_2$ atmosphere. The weight gain of the sample was measured using an analytical balance to determine the percent of $CO_2$ capture. The difference between the initial and final weights was used to understand the conversion reaction:

$$BaCe_{1-x-y}M_xCa_yO_{3-\delta}(s) + CO_2(g) \xrightarrow{800\ °C,\ 12\ h} BaCO_3(s) + Ce_{1-x-y}M_xCa_yO_{2-\delta}(s) \quad (1)$$

After the $CO_2$ reaction was complete, the powders were washed with dilute HCl, then thoroughly washed in water, and dried in air. The product was washed with acid until no further effervescence was observed from $BaCO_3$. The powders were characterized using PXRD. The acid-washed powders of Sm- and (Sm + Ca)-containing $CeO_2$ were then formed into pellets (~1.5 cm diameter and ~0.2 cm thickness) and sintered at 1450 °C for 24−48 h, while the In-doped materials were sintered at 800 °C for 24 h in air for electrical conductivity measurements. Unfortunately, the In-doped $CeO_2$ samples decomposed into $CeO_2$ and $In_2O_3$ at elevated temperatures, and hence we have sintered at much lower temperatures for electrical measurements. Further characterization involved scanning electron microscopy (SEM; JEOL JXA-8200 electron probe microanalyzer, Japan) to determine the surface morphology of the prepared perovskite precursors, $CO_2$ reacted products, acid-washed powders, and sintered products.

**2.3. Electrical Characterization.** Electrical conductivity measurements were performed in air using Pt electrodes. Pt paste (LP A88-11S, Heraeus Inc., Germany) was applied using a paint brush to both sides of the sintered Sm-doped cerate pellets (~1.5 cm diameter and ~0.2 cm thickness) and cured at 1000 °C for 1 h in air to remove the organic binders. The In-doped cerate pellets were cured at 750 °C for 1 h in air to halt any decomposition of the material. Pt wires were attached to the surface of the pellet using a spring-loaded contact, which served as a current collector. The cell was heated to the desired temperature of 400−800 °C using a Barnstead tubular furnace (model 21100) and held at a constant temperature for a minimum of 1 h and a maximum of 48 h prior to each measurement. The alternating current (ac) impedance and gain-phase analyzer (Solartron ac impedance spectroscopy; SI model 1260, 100 mV; 0.01 Hz to 10 MHz) was used to determine the conductivity. A two-probe electrochemical cell was employed for the electrical characterization. The conductivity of each sample was measured during two subsequent heating and cooling cycles to ensure reproducibility of the results.

## 3. Results and Discussion

**3.1. Synthesis of Sm- and (Sm + Ca)-Doped $CeO_2$ Using a $CO_2$ Capture Reaction of the Barium Perovskites.** PXRD analysis shows the formation of perovskite-like $BaCe_{0.9}Sm_{0.1}O_{2.95}$, $BaCe_{0.8}Sm_{0.2}O_{2.9}$, $BaCe_{0.8}Sm_{0.05}Ca_{0.15}O_{2.825}$, $BaCe_{0.9}In_{0.1}O_{2.95}$, and $BaCe_{0.8}In_{0.2}O_{2.9}$. We could index all of the observed diffraction lines based on a perovskite ($ABO_3 \equiv BaCeO_3$)-like cell ($a_p \sim 4$ Å). No additional lines due to unreacted starting materials and potential impurities in the $BaO-CaO-CeO_2-Sm_2O_3$ or $In_2O_3$ systems were observed. The lattice parameters obtained for the perovskites using least-squares refinement are listed in Table 1. The lattice parameters were found to be comparable to those of similar perovskite-like structures reported in the literature.[56−61] $BaCe_{0.9}Sm_{0.1}O_{2.95}$ and $BaCe_{0.8}Sm_{0.2}O_{2.9}$ were found

(56) Chakroborty, A.; Sharma, A. D.; Maiti, B.; Haiti, H. S. *Mater. Lett.* **2002**, *57*, 862–867.
(57) Giannici, F.; Longo, A.; Balerna, A.; Kreurer, K.; Martorana, A. *Chem. Mater.* **2007**, *19*, 5714–5720.
(58) Knight, K. S. *Solid State Ionics* **2000**, *127*, 43–48.
(59) Kunstler, K.; Lang, H.-J.; Maiwald, A.; Tomandl, G. *Solid State Ionics* **1998**, *107*, 221–229.
(60) Ranran, P.; Yan, W.; Lizhai, Y.; Zongqiang, M. *Solid State Ionics* **2006**, *177*, 389–393.
(61) Matshevich, N. I. *J. Therm. Anal. Calorim.* **2007**, *90*, 955–958.

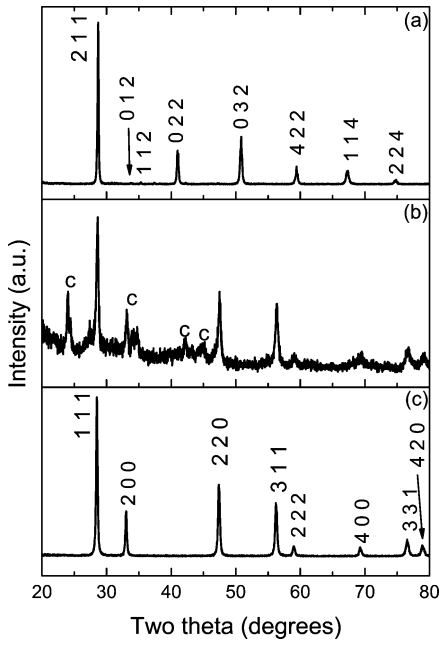


**Figure 1.** PXRD patterns showing the conversion of perovskite-type doped barium cerate into fluorite-type structure oxide ion electrolytes: (a) as-prepared $BaCe_{0.8}Sm_{0.05}Ca_{0.15}O_{2.825}$; (b) sample a heated to 800 °C in $CO_2$ for 12 h; (c) sample b washed with dilute acid and subsequently dried in air. The diffraction lines due to $BaCO_3$ are marked as c in part b.

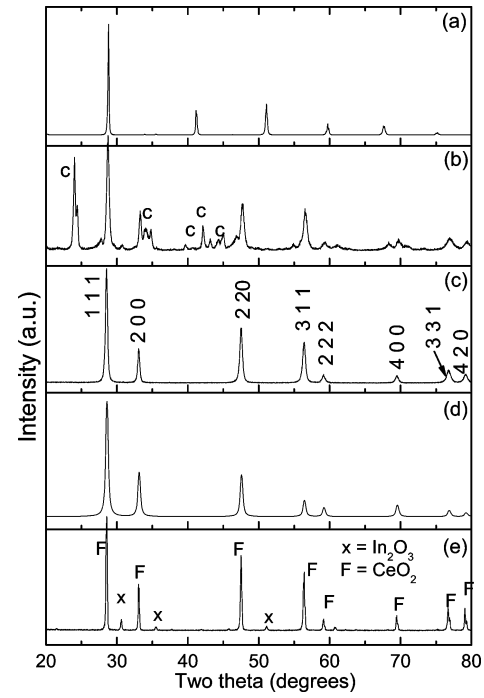


**Figure 2.** PXRD patterns of (a) as prepared perovskite-like structure $BaCe_{0.9}In_{0.1}O_{2.95}$, (b) sample a heated to 800 °C in $CO_2$ for 12 h, (c) sample b treated with dilute acid and subsequently dried in air, (d) theoretical PXRD obtained using $CeO_2$ as the input parameter in a *Powder Cell*, and (e) $Ce_{0.9}In_{0.1}O_{1.95}$ synthesized by the ceramic method at 1500 °C. The diffraction lines due to $BaCO_3$ are marked as c in part b. The biphasic material in part e is clearly shown with X denoting $In_2O_3$ lines and F denoting $CeO_2$ lines.

to crystallize in a simple cubic structure, while $BaCe_{0.8}Sm_{0.05}Ca_{0.15}O_{2.825}$ was found to crystallize in an orthorhombic cell with $2a_p \times \sqrt{2}a_p \times \sqrt{2}a_p$ and is akin to undoped $BaCeO_3$ ($a = 8.779$ Å; $b = 6.214$ Å; $c = 6.236$ Å; Joint Committee on Powder Diffraction Standards (JCPDS) No. 22-0074). The Shannon ionic radii for 6-fold O-coordinated $Sm^{3+}$, $Ca^{2+}$, and $Ce^{4+}$ are 0.964, 1.00, and 0.80 Å, respectively.[62] As the concentration of the Sm dopant increases in $BaCe_{1-x}Sm_xO_{3-\delta}$, the $2\theta$ values decrease, which is the expected trend for Sm substitution. It must be mentioned that a similar observation has been reported for other rare-earth-doped perovskites.[29] The $BaCe_{0.9}In_{0.1}O_{2.95}$ and $BaCe_{0.8}In_{0.2}O_{2.9}$ precursor materials could also be indexed on a perovskite cubic cell with a double perovskite cell of $\sim 2a_p$. All of the barium perovskites that were reacted with $CO_2$ at 800 °C showed a complex diffraction pattern. The amount of weight gain after the $CO_2$ reaction was attributed to the formation of $BaCO_3$, according to the proposed reaction (1). Figure 1 shows the conversion of the barium perovskite $BaCe_{0.8}Sm_{0.05}Ca_{0.15}O_{2.825}$ (Figure 1a) into $BaCO_3$ and a doped cerium fluorite structure (Figure 1b) after reaction with $CO_2$. Similar diffraction patterns were obtained for other investigated materials, including Sm- and In-doped perovskites (Figures 2 and S1−S3 in the Supporting Information).

Virkar and others,[63−75] Irvine and co-workers,[66,67] and many others[55,68,69] recorded similar PXRD patterns of $CO_2$-reacted barium cerates, which agree with this present work. Table 1 lists the theoretical $CO_2$ capture per ceramic gram as well as the experimental capture at 800 °C. It should be noted that the $CO_2$ capture was determined to be larger than 98% for each of the barium perovskites, suggesting that reaction (1) went to completion and all of the Ba atoms in the perovskite lattice have been transformed into $BaCO_3$. Thermodynamic studies of barium cerate materials by Matsumoto et al. showed that carbonate formation is favorable below 1041 °C.[68] Very interestingly, $BaCe_{0.8}Sm_{0.05}Ca_{0.15}O_{2.825}$ showed a $CO_2$ capture value of 0.1423 g per ceramic gram of material, which was only due to the Ba contribution (Table 1). The reaction of $BaCe_{0.8}Sm_{0.05}Ca_{0.15}O_{2.825}$ with $CO_2$ to yield $CaCO_3$ and $BaCO_3$ can be excluded because this would have led to an increased $CO_2$ capture of 0.1642 g per ceramic gram, which was not found experimentally (0.1423 g; Table 1). These results were further confirmed from the PXRD pattern in which the 100% peak

(62) Shannon, R. D. *Acta Crystallogr.* **1976**, *A32*, 751–767.
(63) Gopalan, S.; Virkar, A. V. *J. Electochem. Soc.* **1993**, *140*, 1060–1065.
(64) Tanner, C. W.; Virkar, A. V. *J. Electrochem. Soc.* **1996**, *143*, 1386–1389.
(65) Bhide, S. V.; Virkar, A. V. *J. Electrochem. Soc.* **1999**, *146*, 2038–2044.
(66) Azad, A. K.; Irvine, J. T. S. *Solid State Ionics* **2007**, *178*, 635–640.
(67) Zakowsky, N.; Williamson, S.; Irvine, J. T. S. *Solid State Ionics* **2005**, *176*, 3019–3026.
(68) Matsumoto, H.; Kawasaki, Y.; Ito, N.; Enoki, M.; Ishihara, T. *Electrochem. Solid-State Lett.* **2007**, *10*, B77–B80.
(69) Ryu, K. H.; Haile, S. M. *Solid State Ionics* **1999**, *125*, 355–367.
(70) Zhang, T. S.; Ma, J.; Huang, H. T.; Hing, P.; Xia, Z. T.; Chan, S. H.; Kilner, J. A. *Solid State Sci.* **2003**, *5*, 1505–1511.
(71) Singh, K.; Acharya, S. A.; Bhoga, S. S. *Ionics* **2007**, *13*, 429–434.
(72) Banerjee, S.; Devi, P. S.; Topwal, D.; Mandal, S.; Menon, L. *Adv. Funct. Mater.* **2007**, *17*, 2847–2854.
(73) Pearce, M. C.; Thangadurai, V. *Asian Pac. J. Chem. Eng.*, in press.
(74) Kraus, W.; Nolze, G. J. *Appl. Crystallogr.* **1996**, *29*, 301–303.
(75) Zhang, H.; Wang, J.; Wang, S. C.; Li, Z. C. *Trans. Nonferrous Met. Soc. China* **2007**, *17*, s565–s569.

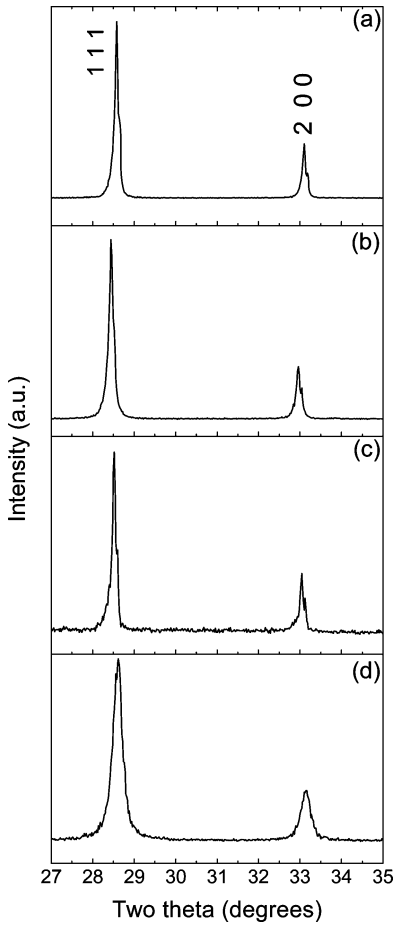


**Figure 3.** Selected region of PXRD patterns of the acid-washed product sintered at 1450 °C for 24 h in air: (a) $Ce_{0.9}Sm_{0.1}O_{1.95}$, (b) $Ce_{0.8}Sm_{0.2}O_{1.9}$, and (c) $Ce_{0.8}Sm_{0.05}Ca_{0.15}O_{1.825}$. For purpose of comparison, the standard $CeO_2$ sample obtained from Alpha is shown in part d. We clearly see a shift in the peak position caused by different concentrations and ionic size of the dopant.

of $CaCO_3$ ($2\theta = 30°$, JCPDS No. 51-1524) is absent but the 100% peak of $BaCO_3$ ($2\theta = 24°$, JCPDS No. 41-0373) is visible (Figure 1b). Hence, Ca in $BaCe_{0.8}Sm_{0.05}Ca_{0.15}O_{2.825}$ does not contribute to the $CO_2$ capture. For comparison, we investigated the stability of starting materials such as CaO, $CeO_2$, $Sm_2O_3$, and $In_2O_3$ under $CO_2$ with the same experimental conditions. We found that pure CaO had about 93% $CO_2$ capture and $CeO_2$ showed no capture while $Sm_2O_3$ and $In_2O_3$ showed negligible capture of 0.9 and 0.1 wt %, respectively, at 800 °C for 12 h. PXRD patterns of $CO_2$-reacted $Sm_2O_3$ and $In_2O_3$ were the same as those of pure $Sm_2O_3$ and $In_2O_3$. However, the $CO_2$-reacted CaO sample gave a more complex $CaCO_3$ pattern. This result clearly confirms that the $CO_2$ capture was determined solely by the Ba atoms in the perovskites and also indicates that materials (for example, CaO) exhibit different physical properties when confined in a lattice in comparison to pure-phase materials.

The $CO_2$-treated powders were washed in acid and water to remove $BaCO_3$. Reaction (2) clearly shows the process that occurred during the acid washing for the $BaCe_{0.8}Sm_{0.05}Ca_{0.15}O_{2.825}$ sample; other materials follow a similar reaction.

$$BaCO_3(s) + Ce_{0.8}Sm_{0.05}Ca_{0.15}O_{1.825}(s) \xrightarrow{HCl} BaCl_2(aq) + Ce_{0.8}Sm_{0.05}Ca_{0.15}O_{1.825}(s) + CO_2(g)\uparrow \quad (2)$$

It is anticipated that the resultant product after acid washing would be a fluorite-type material. The complete syntheses starting with the perovskite-like material (Figure 1a), $CO_2$-reacted material (Figure 1b), and acid-washed product (Figure 1c) are shown in Figure 1 for the $x = 0.05$, $y = 0.15$ member of $BaCe_{1-x-y}Sm_xCa_yO_{3-\delta}$. We clearly see that the perovskite peaks at $2\theta \approx 41°$, 51°, 59°, 67°, and 75° are absent in the acid-washed product, suggesting that the parent barium perovskite material has been converted into the fluorite-type cerate. The fluorite samples were indexed with space group $Fm\bar{3}m$ (No. 225), and the shift in the (111) and (200) $CeO_2$ peaks with different $Sm_2O_3$ concentrations is shown in Figure 3 (Table 2). Because the 8-fold O-coordinated ionic radius of $Sm^{3+}$ (1.079 Å) is larger than the ionic radius of $Ce^{4+}$ (0.97 Å), the d spacing was found to increase as the concentration of the Sm dopant increased.[62] For comparison, we also included undoped $CeO_2$ ($a = 5.411$ Å) in Figure 3d. The lattice parameters of the 1450 °C Sm-doped sintered samples were determined to be $a = 5.4162(7)$ Å for $Ce_{0.9}Sm_{0.1}O_{1.95}$, $a = 5.4298(8)$ Å for $Ce_{0.8}Sm_{0.2}O_{1.9}$, and $a = 5.4199(7)$ Å for $Ce_{0.8}Sm_{0.05}Ca_{0.15}O_{1.825}$.

The theoretical lattice parameter of doped fluorites can be obtained using the formula[70]

$$a = \frac{4}{\sqrt{3}}[xr_{Sm} + (1-x)r_{Ce} + (1-0.25x)r_O + 0.25xr_{Vo}] \times 0.9971 \quad (3)$$

where $x$ is the Sm or In content ($0 \le x \le 0.4$) in $Ce_{1-x}M_xO_{2-\delta}$. The ionic radius values were taken from the literature,[70] where the $Sm^{3+}$ ionic size is $r_{Sm} = 1.079$ Å, the $Ce^{4+}$ ionic size is $r_{Ce} = 0.97$ Å, the $O^{2-}$ ionic size is $r_O = 1.38$ Å, and the oxygen vacancy radius is $r_{Vo} = 1.164$ Å.[70] Figure 4 shows the expected theoretical lattice parameters of Sm-, Ca-, and In-doped $CeO_2$ for the range $0 \le x \le 0.4$. Very interestingly, the lattice parameters of the acid-washed and 1450 °C sintered Sm-doped samples are consistent with Sm-doped $CeO_2$ reported in the literature[38,39,71,72] and also fall very close to the expected values obtained using eq 3.[70] Goodenough et al.[82] and Fu et al.[29] reported a similar trend for rare-earth-doped $CeO_2$.

**Table 2.** Lattice Parameters for 1450 °C Sintered Sm- and (Ca + Sm)-Doped $CeO_2$ Samples and Their Conductivity and Activation Energy

| compound | lattice parameter (Å) | $\sigma_{bulk}$ (S/cm) 510 °C | $\sigma_{bulk}$ (S/cm) 610 °C | $E_a$ (eV) (>600 °C) |
|---|---|---|---|---|
| $Ce_{0.9}Sm_{0.1}O_{1.95}$ | 5.4162(7) | $2.7 \times 10^{-3}$ | $4.3 \times 10^{-3}$ | 0.94 |
| $Ce_{0.8}Sm_{0.2}O_{1.9}$ | 5.4298(8) | $4.1 \times 10^{-3}$ | $8.7 \times 10^{-3}$ | 0.75 |
| $Ce_{0.8}Sm_{0.2}O_{1.9}$(ceramic) | 5.4361(2) | $3.9 \times 10^{-3}$ | $7.0 \times 10^{-3}$ | 0.65 |
| $Ce_{0.8}Sm_{0.05}Ca_{0.15}O_{1.825}$ | 5.4199(7) | $4.0 \times 10^{-3}$ | $8.5 \times 10^{-3}$ | 0.66 |

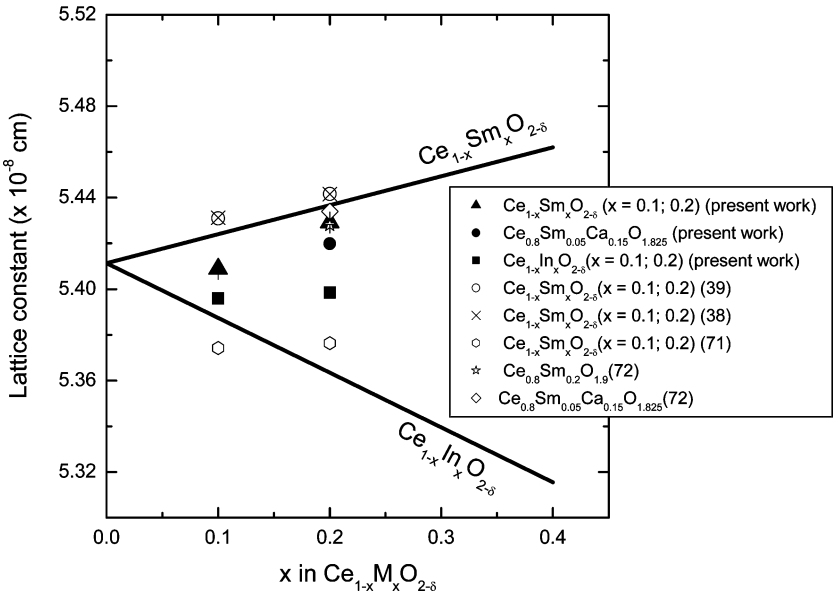


**Figure 4.** Comparison of the experimental lattice constants of Sm-, (Sm + Ca)-, and In-doped $CeO_2$ with theoretically calculated lattice parameters and literature values.

**3.2. Stabilization of In-Doped $CeO_2$ via a $CO_2$ Capturing Technique.** A large number of chemical substitutions in $CeO_2$ have been reported in order to understand the role of the dopant on the composition−structure−electrical conductivity relationship of cerates.[21,29−39] On the basis of the Shannon ionic radii difference between $In^{3+}$ and $Ce^{4+}$, one would expect to substitute In for Ce in the fluorite structure.[62] However, our earlier and recent attempt to prepare 10 and 20% In-substituted $CeO_2$ by ceramic reactions at 1000 °C (24 h) and 1500 °C (24 h) showed the formation of a biphasic product containing $CeO_2$ and $In_2O_3$.[73] Very interestingly, we are able to prepare In-doped $CeO_2$ materials using the corresponding barium perovskite using the $CO_2$ reaction and subsequent acid washing (Figures 2 and S3 in the Supporting Information). For example, the perovskite-type In-doped $BaCe_{0.9}In_{0.1}O_{2.95}$ was first prepared by solid-state reaction and then treated subsequently with $CO_2$ at 800 °C for 12 h. The amount of $CO_2$ gain in the reaction was consistent with proposed reaction (4).

$$BaCe_{1-x}In_xO_{3-\delta}(s) + CO_2(g) \xrightarrow{800\ ^\circ C,\ 12\ h} BaCO_3(s) + Ce_{1-x}In_xO_{2-\delta}(s) \quad (4)$$

The acid-washed product PXRD pattern shows a fluorite-type structure (Figures 2c and S3c in the Supporting Information; $a$ = 5.4066(5) Å for $Ce_{0.9}In_{0.1}O_{1.95}$, $a$ = 5.4062(5) Å for $Ce_{0.8}In_{0.2}O_{1.9}$). We have calculated the theoretical PXRD patterns for 10 and 20% In-substituted $CeO_2$ samples using the parent $CeO_2$ structure data in the *Powder Cell* program (Figures 2d and S3d in the Supporting Information).[74] We see that both measured and calculated PXRD patterns match very well. Figure 2e also includes the PXRD pattern of $Ce_{0.9}In_{0.1}O_{1.95}$ prepared using the ceramic method and sintered at 1500 °C. It is evident that the material is biphasic, comprised of $CeO_2$ and $In_2O_3$ (JCPDS Nos. 06-0416 and 22-0336) diffraction lines. The lattice parameters for the 800 °C sintered In-doped cerates prepared via $CO_2$ capture were determined to be $a$ = 5.398(1) Å for $Ce_{0.9}In_{0.1}O_{1.95}$ and $a$ = 5.393(2) Å for $Ce_{0.8}In_{0.2}O_{1.9}$ (Table 3). This is expected because the ionic radius of $In^{3+}_{(VIII)}$ = 0.92 Å is smaller than that of $Ce^{4+}_{(VIII)}$ = 0.97 Å.[62]

**Table 3.** Lattice Parameters for In-Doped $CeO_2$ Samples and Their Conductivity and Activation Energy

| compound | lattice parameter (Å) | $\sigma_{500\ ^\circ C}$ (S/cm) | $\sigma_{600\ ^\circ C}$ (S/cm) | $E_a$ (eV) |
|---|---|---|---|---|
| $Ce_{0.9}In_{0.1}O_{1.95}$[a] | 5.398(1) | $2.4 \times 10^{-7}$ | $2.0 \times 10^{-6}$ | 1.25 (350−750 °C) |
| $Ce_{0.8}In_{0.2}O_{1.9}$[a] | 5.393(1) | $3.3 \times 10^{-7}$ | $2.8 \times 10^{-6}$ | 1.42 (350−750 °C) |
| $Ce_{0.9}In_{0.1}O_{1.95}$[b] | composite | $5.4 \times 10^{-5}$ | $2.8 \times 10^{-4}$ | 1.15 (250−850 °C) |
| $Ce_{0.8}In_{0.2}O_{1.9}$[b] | composite | $4.2 \times 10^{-4}$ | $1.8 \times 10^{-3}$ | 1.00 (250−850 °C) |
| $CeO_2$[c] | 5.411 | $1.2 \times 10^{-7}$ | $1.8 \times 10^{-6}$ | 1.64 (350−800 °C) |

[a] Total conductivity values for single-phase materials (800 °C sintered samples). [b] Bulk conductivity values for composite materials (1500 °C sintered samples). [c] Reference 70.

Zhang et al. have recently claimed to prepare single-phase fluorite-type $Ce_{0.9}In_{0.1}O_{1.95}$ by polymerization and sintering at 1450 °C;[75] however, we were not able to prepare single-phase fluorites using the ceramic method at the same temperature. In order to understand the thermodynamic stability of the present In-doped cerates prepared via the $CO_2$ capture technique, the acid-washed products were sintered at 500, 600, 700, 800, 900, 1000, and 1200 °C for 24 h in air. Surprisingly, we have found that below 800 °C the material consists of a single-phase fluorite phase and at 900 °C the composite material of $In_2O_3$ and $CeO_2$ was formed (Figures 5 and S4 in the Supporting Information). The PXRD stability study shown in Figure 5 clearly shows $In_2O_3$ precipitation from the lattice above 800 °C. The contribution of $In_2O_3$ was also found to increase with an increase in the sintering temperature, and the intensity of the $In_2O_3$ peaks at 1200 °C are more obvious than that at 900 °C. $In_2O_3$ has a 100% line at $2\theta \approx 30.6°$ (JCPDS No. 06-0416), which is evident in Figure 5. These results suggest that In-doped samples appear to be thermodynamically unstable at elevated temperatures. Therefore, both the $Ce_{0.9}In_{0.1}O_{1.95}$ and $Ce_{0.8}In_{0.2}O_{1.9}$ samples can be considered as having a "metastable"

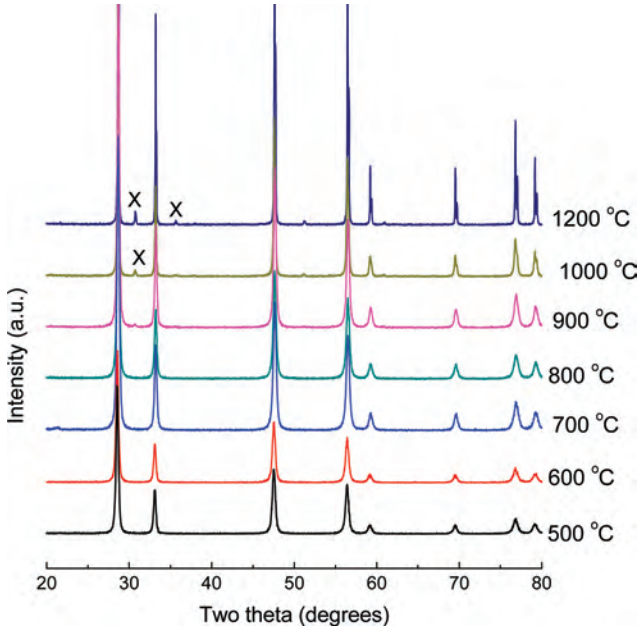


**Figure 5.** PXRD patterns showing the metastability of $Ce_{0.9}In_{0.1}O_{1.95}$ prepared by the $CO_2$ capture method at 500, 600, 700, 800, 900, 1000, and 1200 °C. The lines marked by X denote diffraction lines due to $In_2O_3$ (JCPDS No. 06-0416).

phase, existing as a single-phase fluorite structure at low temperatures. This proves our findings that In-doped cerates cannot be prepared after sintering at high temperatures. Very interestingly, attempts to prepare $Ce_{0.9}In_{0.1}O_{1.95}$ and $Ce_{0.8}In_{0.2}O_{1.9}$ via the ceramic method and sintering at 800 °C for 24 h yield PXRD patterns that consist of a biphasic material (Figure S5 in the Supporting Information). Therefore, the $CO_2$ capture technique may be the only viable means to incorporate indium into a fluorite lattice.

Figure 6 shows the variation in the lattice parameter as a function of the sintering temperature of In-doped $CeO_2$. The lattice parameter decreases slightly as the sintering temperature increases up to 800 °C; above this temperature, the lattice parameter increases, approaching the lattice parameter of $CeO_2$ (5.411 Å).[70] The increase in the lattice constant above 800 °C is expected as the material loses $In_2O_3$ from the lattice to give a material that resembles $CeO_2$. The decrease in the lattice parameter with increasing temperature is known for many ceramic materials including Ti-doped $PbZrO_3$,[76] Gd-doped $CeO_2$,[46] a fluorite-type phase in the Ce−Gd−Mn−O system,[77] and $Ce-La_{0.9}Sr_{0.1}Ga_{0.8}Mg_{0.2}O_{3-\delta}$ (LSGM).[77b] The apparent density of the sintered Sm-doped cerates was determined (using mass by volume) to be more than 80% of the theoretical density. The density of the In-doped cerates was determined to be about 41% of the theoretical density due to the low sintering temperature, as anticipated.

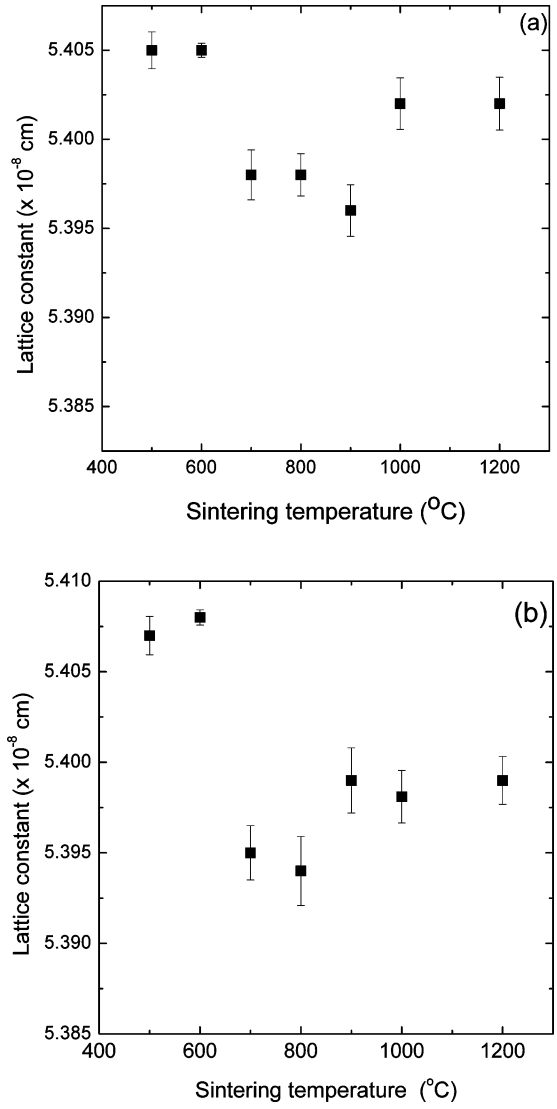


**Figure 6.** Variation of the lattice constant as a function of the sintering temperature for (a) $Ce_{0.9}In_{0.1}O_{1.95}$ and (b) $Ce_{0.8}In_{0.2}O_{1.9}$ prepared from the perovskite using the $CO_2$ capture technique.

The proposed conversion of a perovskite-like phase into a fluorite phase was explained using a simple cubic perovskite in Figure 7. Recently, Malavasi et al. have reported the crystal structure of Y-doped $BaCeO_3$ at a variety of temperatures.[78] They found that between room temperature and 400 °C the perovskite material is monoclinic (*I*2/*m*), at 500 °C the material is orthorhombic (*Imma*), at 600 and 700 °C it is rhombohedral (*R*3*c*), and at 800 °C the material is cubic with a space group of $Pm\bar{3}m$. In a simple primitive cubic $ABO_3$ perovskite, A, B, and O cations occupy 1a, 1b, and 3c Wyckoff positions, respectively, in the space group $Pm\bar{3}m$ (space group number 221, $z = 1$, where $z$ is the number of formula units in a unit cell)[79] The fluorite structure has a face-centered-cubic (fcc) lattice in which $Ce^{4+}$ and $O^{2-}$ ions occupy the 4a and 8c Wyckoff positions, respectively, in

(76) Lucuta, P. G. R.; Constantinescu, F. L.; Barb, D. *J. Am. Ceram. Soc.* **1985**, *68*, 533–537.
(77) (a) Sadykov, V. A.; Borchert, Yu. V.; Alikina, G. M.; Lukashevich, A. I.; Mezentseva, N. V.; Muzykantov, V. S.; Moroz, E. M.; Rogov, V. A.; Zaikovskii, V. I.; Zyuzin, D. A.; Uvarov, N. F.; Ishchenko, A. V.; Zyryanov, V. V.; Smirnova, A. *Glass Phys. Chem.* **2007**, *33*, 320–334. (b) Zhang, X.; Ohara, S.; Maric, R.; Okawa, H.; Fukui, T.; Yoshida, H.; Inagaki, T.; Miura, K. *Solid State Ionics* **2000**, *133*, 153–160.
(78) Malavasi, L.; Ritter, C.; Chiodelli, G. *Chem. Mater.* **2008**, *20*, 2343–2351.
(79) Thomas, N. W. *Acta Crystallogr.* **1998**, *B54*, 585–599.

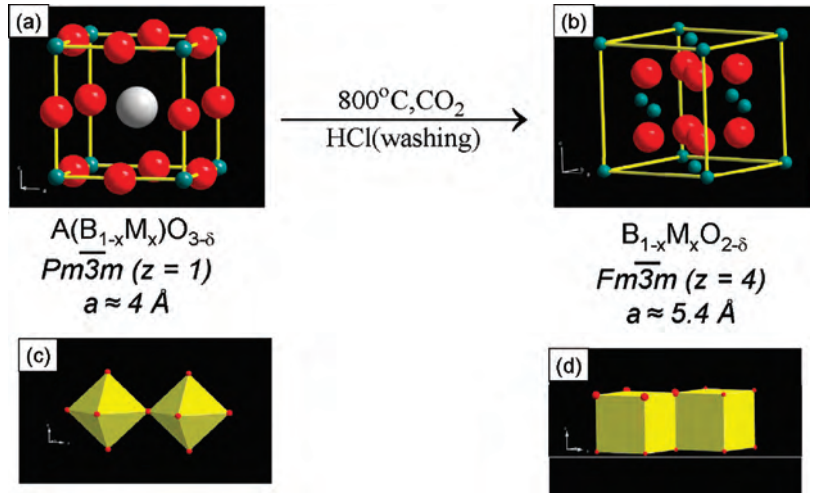


**Figure 7.** Idealized schematic representation showing the conversion of a perovskite-like structure (a and c) into a fluorite-type structure (b and d). One formula unit of the simple cubic perovskite $ABO_3$ may yield $^1/_4$ of the fluorite $BO_2$ structure.

space group $Fm\bar{3}m$ (space group number 225, $z = 4$).[80] We believe that the A-site cation ($Ba^{2+}$) and one of the $O^{2-}$ ions in the perovskite may combine with $CO_2$ to form $BaCO_3$, and subsequently, the remaining B-site cations ($In^{3+}$, $Ce^{4+}$, and $Sm^{3+}$) and two O atoms (per formula unit) rearrange into a fluorite-type structure. The Ce−O bond length in a cubic perovskite $BaCeO_3$ is ~2.22 Å, while the Ce−O bond length is slightly longer, ~2.35 Å, in the fluorite phase. This suggests that, during the phase transformation reaction with $CO_2$, metal−oxygen bonds may be broken and formed. A fluorite has four formula units per unit cell, and a perovskite has one formula unit per unit cell. Accordingly, it is anticipated that four simple cubic unit cells of perovskite material are required to produce one unit cell of fluorite material.

Figure 8 shows SEM images of the prepared materials. Figure 8a shows the barium perovskite material $BaCe_{0.8}Sm_{0.2}O_{2.9}$, and Figure 8b shows the $CO_2$ reaction product after reaction (2) was completed. Figure 8c shows the acid-washed product, and Figure 8d shows the 1450 °C sintered $Ce_{0.8}Sm_{0.2}O_{1.9}$ material. It can be seen that the sintered material has large aggregates of particles caused by crystal growth. Grain boundaries are also visible in the sintered product. Similar SEM images were observed for 10% Sm- and (Ca + Sm)-doped $CeO_2$, and characterization of the In-doped samples will be investigated in future work.

**3.3. Electrical Conductivity. 3.3.1.. ac Impedance Analysis of Doped $CeO_2$.** Figure 9 shows the typical resistivity plots of $Ce_{0.9}Sm_{0.1}O_{1.95}$ prepared by the $CO_2$ capture method at 320, 492, and 784 °C in air using Pt electrodes. All of the Sm- and (Sm + Ca)-doped samples show similar impedance plots.[55,81−88] The contributions due to bulk (b), grain-boundary (gb), and electrode (e) effects were observed at high, intermediate, and low frequencies, respectively, especially at low temperatures. Capacitance values were obtained using the formula $\omega RC = 1$ (where $\omega = 2\pi F$ and $F$ is the maximum ac frequency of the semicircle). The capacitance for the high-frequency semicircle at 320 °C was determined to be $\sim 5.72 \times 10^{-11} F$. This value is typical for the bulk contribution in ceramics due to ionic conductivity.[83] At high temperatures, we see a clear intercept at the real axis at low frequencies, while at low temperatures, only a part of the semicircle was observed. This was because low-frequency measurements (less than 0.01 Hz) were not conducted. The appearance of a low-frequency intercept to the real axis indicates the nonblocking nature of the electrode and electrolyte interfaces, which is consistent with the application of porous Pt electrodes.[83,89] Furthermore, the Sm- and (Sm + Ca)-doped materials exhibit mainly oxide ion conductivity at high oxygen partial pressures.[32,34] It must be mentioned that we were not able to resolve the grain-boundary and electrode contributions successfully over the entire temperature range investigated because of an overlap of the semicircles at high temperatures. In order to understand the chemical composition−structure−electrical conductivity relationship of the materials synthesized using the $CO_2$ capture method, we uniformly took the high-frequency intercept or minimum to the real axis to determine the bulk conductivity value. Furthermore, the bulk conductivity of materials is routinely used in the literature to understand the functional properties of materials. For any given sample, we found that the impedance plots were highly reproducible during the two subsequent heating and cooling cycles and from one batch of samples to another. The

(80) Haisa, M. *Acta Crystallogr.* **1982**, *A38*, 443–453.
(81) Balazs, G. B.; Glass, R. S. *Solid State Ionics* **1995**, *76*, 155–162.
(82) Goodenough, J. B.; Ruiz-Diaz, J. E.; Zhen, Y. S. *Solid State Ionics* **1990**, *44*, 21–31.
(83) Irvine, J. T. S.; Sinclair, D. C.; West, A. R. *Adv. Mater.* **1990**, *2*, 132–138.
(84) Huang, K.; Tichy, R. S.; Goodenough, J. B. *J. Am. Ceram. Soc.* **1998**, *81* (10), 2565–2575.
(85) Huang, K.; Feng, M.; Goodenough, J. B. *J. Am. Ceram. Soc.* **1996**, *79*, 1100–1104.
(86) Tschope, A.; Kilassonia, S.; Birringer, R. *Solid State Ionics* **2004**, *173*, 57–61.
(87) Huang, W.; Shuk, P.; Greenblatt, M.; Croft, M.; Chen, F.; Liu, M. *J. Electrochem. Soc.* **2000**, *147*, 4196–4202.
(88) Dudek, M.; Bogusz, W.; Zych, L.; Trybalska, B. *Solid State Ionics* **2008**, *179*, 164–167.
(89) Armstrong, R. D.; Todd, M. In *Solid State Electrochemistry*; Bruce, P. G., Ed.; Cambridge University Press: Cambridge, U.K., 1995; pp 264−291.

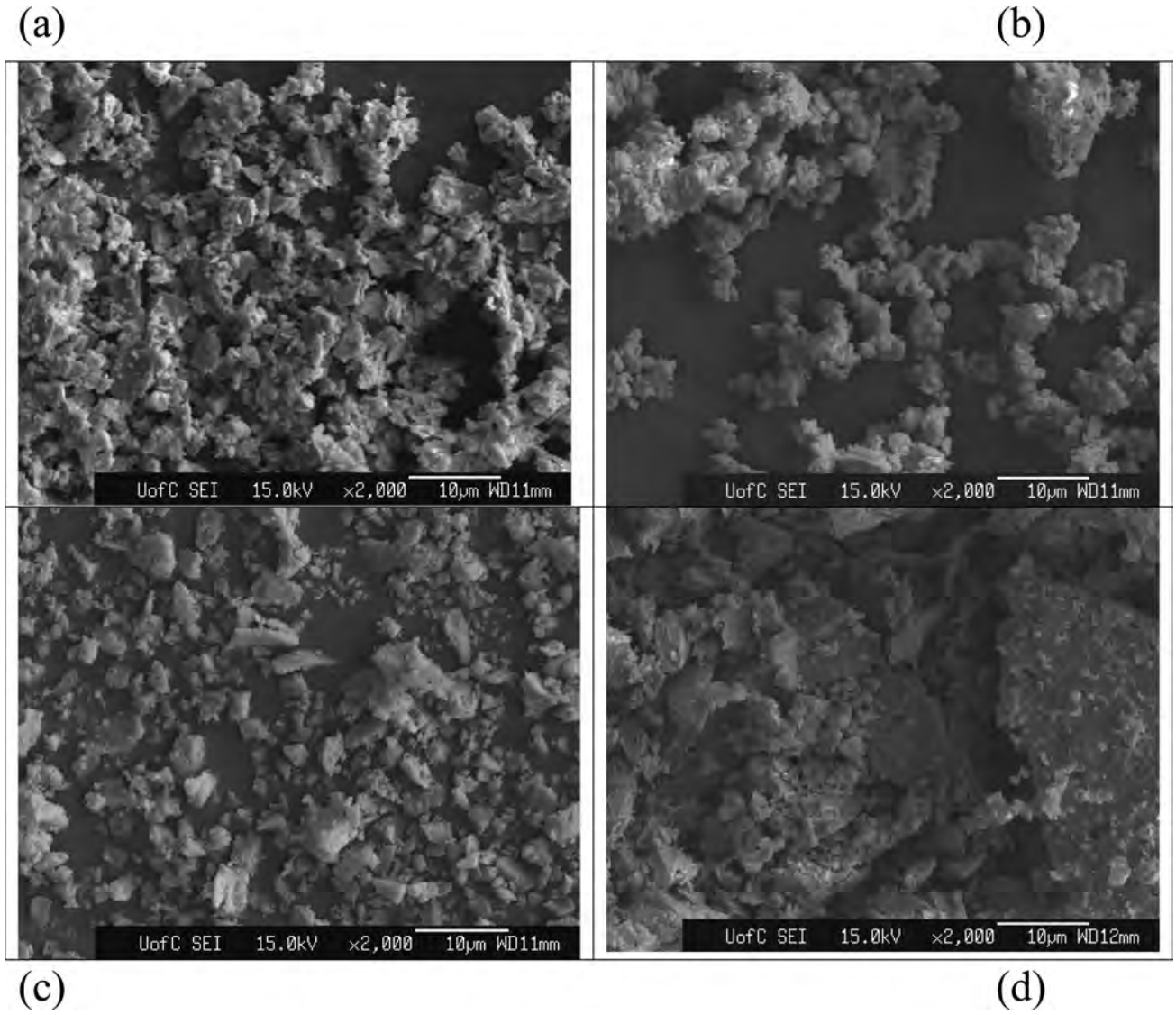


**Figure 8.** SEM images of Sm-doped materials using the $CO_2$ capture technique: (a) as-prepared $BaCe_{0.8}Sm_{0.2}O_{2.9}$ material; (b) sample a heated to 800 °C in $CO_2$ for 12 h; (c) sample b washed with dilute acid and subsequently dried in air to yield the fluorite $Ce_{0.8}Sm_{0.2}O_{1.9}$; (d) 1450 °C sintered $Ce_{0.8}Sm_{0.2}O_{1.9}$.

appearance of positive $Z''$ values in the high-temperature impedance plots indicates the presence of inductive effects (Figure 9c), which is quite commonly reported in the literature.

Figure 10 shows the typical resistivity plots of $Ce_{0.8}In_{0.2}O_{1.9}$ (prepared by the $CO_2$ capture method) at 510, 610, and 710 °C in air using Pt electrodes in the frequency range 0.01 Hz to 10 MHz. Both the 10 and 20% In-doped samples show similar impedance plots over the investigated temperature range. Unlike Sm- and (Sm + Ca)-doped samples, a large overlap of bulk and grain-boundary contributions was observed over the entire investigated temperature range of 400−750 °C for In-doped $CeO_2$ synthesized by the low-temperature $CO_2$ capture method. This may be attributed to poor density (about 41% of the theoretical density) as a result of the low-temperature sintering. Our attempt to increase the density by high-temperature sintering failed because of the lack of high-temperature thermodynamic stability (Figures 5 and S4 in the Supporting Information). It is interesting to note that the composite materials prepared at 1500 °C clearly show bulk, grain-boundary, and electrode contributions (Figure S6 in the Supporting Information) and the impedance plots are similar to those of single-phase (Ca + Sm)- and Sm-doped $CeO_2$. Accordingly, we have calculated the total conductivity (bulk + grain boundary + electrode) using the low-frequency intercept for the single-phase In-doped cerates prepared via the $CO_2$ capture method, while the bulk conductivity was determined for the composite materials from the high-frequency intercept/minimum to the real axis.

**3.3.2.. Ionic Conductivity of Sm- and (Sm + Ca)-Doped $CeO_2$, $Ce_{0.9}In_{0.1}O_{1.95}$, and $Ce_{0.8}In_{0.2}O_{1.9}$.** Figure 11 shows the Arrhenius plots for the electrical conductivity data of $Ce_{0.9}Sm_{0.1}O_{1.95}$, $Ce_{0.8}Sm_{0.2}O_{1.9}$, and $Ce_{0.8}Sm_{0.05}Ca_{0.15}O_{1.825}$ prepared by the $CO_2$ capture method. The bulk ionic conductivity data obtained during the heating and cooling runs were found to follow the same curve, suggesting equilibrium behavior. Between the 0.1 and 0.2 members, the $x = 0.2$ member exhibits a slightly higher ionic

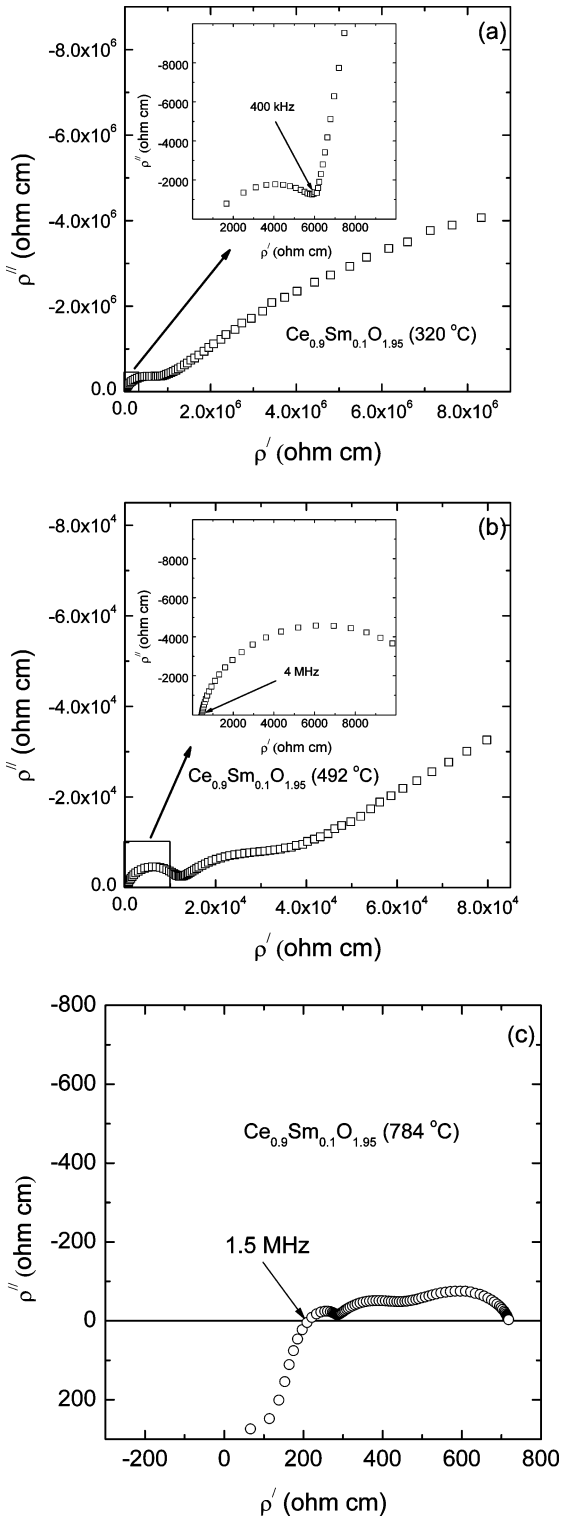


**Figure 9.** ac impedance plots of $Ce_{0.9}Sm_{0.1}O_{1.95}$ prepared by $CO_2$ capture in air using Pt electrodes at (a) 320 °C, (b) 492 °C, and (c) 784 °C. Contributions of the bulk, grain-boundary, and electrode effects are visible at high-, intermediate-, and low-frequency regions, respectively, at low temperatures.

conductivity than the $x = 0.1$ member at high temperatures. Among the samples studied, coupled doping of trivalent $Sm^{3+}$ and divalent $Ca^{2+}$ in $Ce_{0.8}Sm_{0.05}Ca_{0.15}O_{1.825}$ exhibits a slightly higher ionic conductivity over the entire temperature range than $Ce_{0.8}Sm_{0.2}O_{1.9}$ does. We clearly

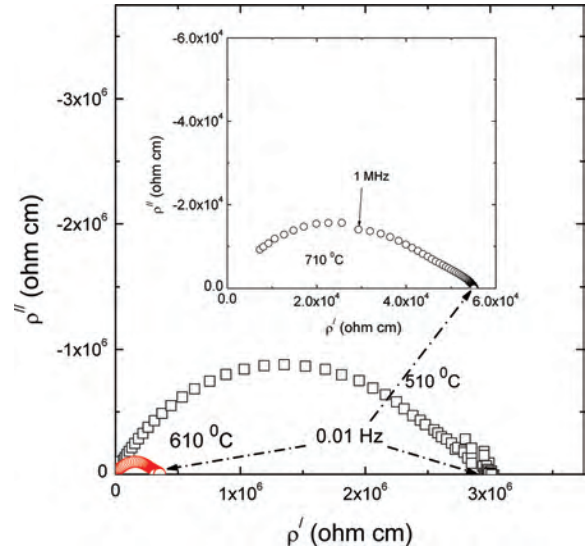


**Figure 10.** ac impedance plots for $Ce_{0.8}In_{0.2}O_{1.9}$ prepared by the $CO_2$ capture method in ambient air using Pt electrodes at (a) 510 °C, (b) 610 °C, and (c) 710 °C, within the frequency range 0.01 Hz to 10 MHz.

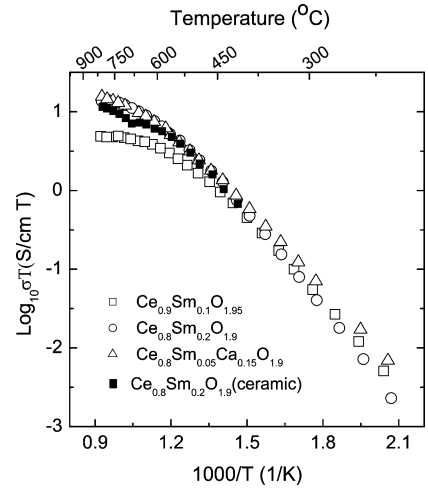


**Figure 11.** Arrhenius plots showing the electrical conductivity of $Ce_{0.9}Sm_{0.1}O_{1.95}$, $Ce_{0.8}Sm_{0.2}O_{1.9}$, and $Ce_{0.8}Sm_{0.05}Ca_{0.15}O_{1.825}$ prepared by the $CO_2$ capture method. For comparison, the electrical conductivity of ceramic (solid state) synthesized $Ce_{0.8}Sm_{0.2}O_{1.9}$ is included. The conductivities of ceramic and $CO_2$-capture-prepared $Ce_{0.8}Sm_{0.2}O_{1.9}$ were found to be nearly the same, suggesting that the latter method yields doped $CeO_2$.

see that the doped samples prepared in the present work have a higher electrical conductivity than pure $CeO_2$ and the conductivity values fall within the range known for similar compositions reported in the literature (Figure 12).[32,90]

The high ionic conductivity of doped $CeO_2$ generally depends on the aliovalent dopant concentration, which determines the oxygen ion vacancies in the lattice. For trivalent, rare-earth ions, a dopant concentration of $x = 0.2$ in $Ce_{1-x}M_xO_{2-\delta}$ gives the maximum conductivity,[36] and for divalent ions, including Ca and Sr, it was found to be around $x = 0.1$.[37] The high ionic conductivity of $Ce_{0.8}Sm_{0.05}Ca_{0.15}O_{1.825}$ compared to those of Sm-doped compounds may be due to an increase in the concentration of oxide ion

(90) Mori, T.; Wang, Y.; Drennan, J.; Auchterlonie, G.; Li, J.; Ikegami, T. *Solid State Ionics* **2004**, *175*, 641–649.

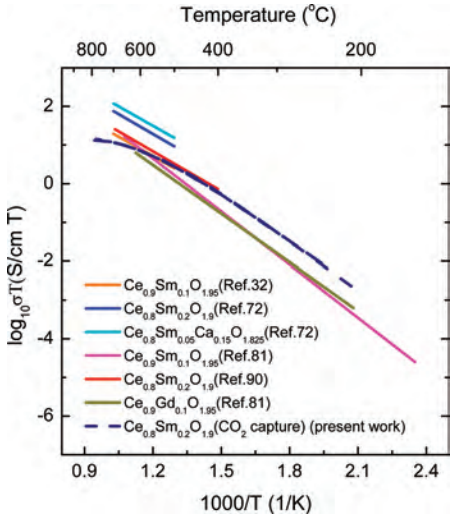


**Figure 12.** Comparison of the Arrhenius plots of $Ce_{0.8}Sm_{0.2}O_{1.9}$ prepared by $CO_2$ capture with previously reported values for similar compositions.

vacancies. Also, this can be explained using the differences in the ionic radii between parent and doped cations. The ionic radii of 8-fold oxygen coordination for $Ca^{2+}$ and $Sm^{3+}$ are 1.12 and 0.97 Å, respectively.[62] The slight enhancement in the ionic conductivity of the Ca- and Sm-doped samples is in agreement with the findings of Banerjee et al. and is also consistent with an increase in the oxide ion vacancy concentrations.[72] For $Ce_{0.9}Sm_{0.1}O_{1.95}$, there were $1.26 \times 10^{21}$ vacancies/cm$^3$, for $Ce_{0.8}Sm_{0.2}O_{1.9}$ there were $2.5 \times 10^{21}$ vacancies/cm$^3$, for $Ce_{0.8}Sm_{0.05}Ca_{0.15}O_{1.825}$ there were $4.4 \times 10^{21}$ vacancies/cm$^3$, for $Ce_{0.9}In_{0.1}O_{1.95}$ there were $1.27 \times 10^{21}$ vacancies/cm$^3$, and for $Ce_{0.8}In_{0.2}O_{1.9}$ there were $2.55 \times 10^{21}$ vacancies/cm$^3$.

The Arrhenius plots for $Ce_{0.9}In_{0.1}O_{1.95}$ and $Ce_{0.8}In_{0.2}O_{1.9}$ prepared by the low-temperature $CO_2$ capture technique and high-temperature sintered composite materials are shown in parts a and b of Figure 13, respectively. The total conductivity of the samples sintered at 800 °C is found to be about 1.5 orders of magnitude lower than those of the bulk conductivity of high-temperature sintered composite materials over the investigated temperature range. From the impedance plot, one could not determine the total conductivity of the composite materials because we did not see a low-frequency intercept to the real axis in the same frequency region. Therefore, we are unable to directly compare the bulk and total conductivity data between the single-phase and composite materials.

It is noteworthy to mention that the electrical conductivity of solid electrolytes, including doped $CeO_2$, changes significantly with the sintering temperature, synthesis conditions, and morphology or particle size.[91−99] For example, Tschöpe et al. recently reported that nanosized $CeO_2$ has about 2

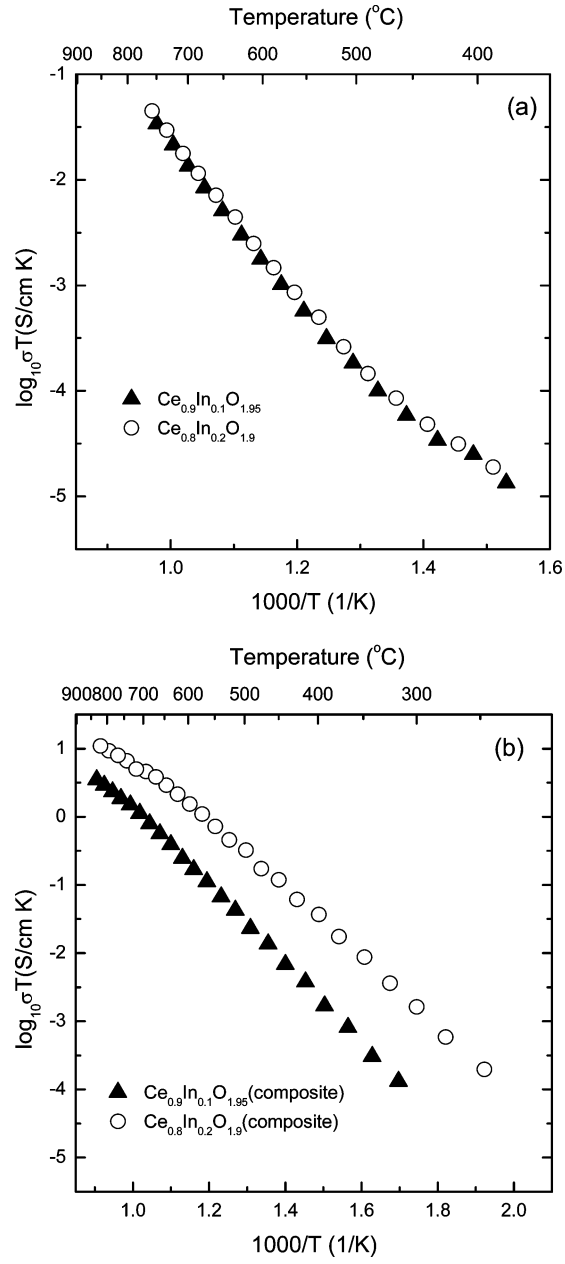


**Figure 13.** Comparison of Arrhenius plots of $Ce_{0.9}In_{0.1}O_{1.95}$ and $Ce_{0.8}In_{0.2}O_{1.9}$ prepared (a) using $CO_2$ capture sintering at 800 °C and (b) using the ceramic method and sintering at 1500 °C.

orders of magnitude lower conductivity compared to micro-sized particles of the same composition.[91,92] Tian et al. reported about 2 orders lower electrical conductivity for doped $CeO_2$ sintered at 700 °C compared to those sintered at 1200 °C.[47] Furthermore, our recent investigation of Y-doped $CeO_2$ prepared by the $CO_2$ capture method showed nanoparticles for the acid-washed materials, and growth of the particles was observed after high-temperature sintering.[55] It is anticipated that low-temperature sintered In-doped $CeO_2$ materials may be present in the nanosize, while high-

(91) Tschöpe, A.; Sommer, E.; Birringer, R. *Solid State Ionics* **2001**, *139*, 255–265.
(92) Tschöpe, A. *Solid State Ionics* **2001**, *139*, 267–280.
(93) Tuller, H. L. *Solid State Ionics* **2000**, *131*, 143–157.
(94) Kim, S.; Maier, J. *J. Electrochem. Soc.* **2002**, *149*, J73–J83.
(95) Kosacki, I.; Suzuki, T.; Petrovsky, V.; Anderson, H. U. *Solid State Ionics* **2000**, *136−137*, 1225–1233.
(96) Li, J.; Ikegami, T.; Mori, T. *Acta Mater.* **2004**, *52*, 2221–2228.
(97) Kleinlogel, C.; Gauckler, L. J. *Solid State Ionics* **2000**, *135*, 567–573.
(98) Zhou, Z.; Huebner, W.; Kosacki, I.; Anderson, H. U. *J. Am. Ceram.Soc.* **2002**, *85* (7), 1757–1762.
(99) Wang, D. Y.; Park, D. D.; Griffith, J.; Nowick, A. S. *Solid State Ionics* **1981**, *2*, 95–105.

temperature sintered composite materials have microsize particles. Low conductivities of the 800 °C sintered In-doped cerates are expected because of the affect of the sintering temperature and particle size. As one could see from the SEM images of doped $CeO_2$ (Figure 8), the sample sintered at 1450 °C shows the presence of microsized particles. Hence, the low conductivity of the low-temperature phase may be attributed to poorly connected particles while the high-temperature composite phases are expected to have good particle contacts. Future work has been planned to study the detailed microstructure and morphology of the metastable as well as other doped $CeO_2$ materials prepared in this study as a function of the sintering temperature. The conductivity of the low-temperature phase is therefore a function of both the sintering temperature and the particle size.

The activation energy for electronic conduction was calculated by fitting the Arrhenius plots using the Arrhenius equation:

$$\sigma T = A \exp\left(-\frac{E_a}{kT}\right) \quad (5)$$

where $A$ is the preexponential factor, $E_a$ is the activation energy, $k$ is Boltzmann's constant ($1.38 \times 10^{-23}$ J/K), and $T$ is the temperature in Kelvin. All of the materials investigated showed Arrhenius behavior at low temperatures and observed a slight change in the slope at higher temperatures. We have obtained two activation energies for the low- and high-temperature regions for Sm- and (Sm + Ca)-doped $CeO_2$. At high temperatures, the ion transport mechanism of the oxide ions changes and therefore the material properties at high temperatures differ from those at low temperatures. In the high-temperature regime, the activation energy was found to be considerably lower than that in the low-temperature regime. The change in the slope in the Arrhenius plot corresponds to a critical temperature of about 560 °C. At this point, the dopant ions act as nucleating centers for the formation of ordered vacancy clusters. At high temperatures, the vacancies are more disordered, and therefore an oxide ion can easily migrate through the lattice. At temperatures lower than the critical temperature, the oxygen vacancies form clusters that inhibit ion migration. Such a change in the slope of the Arrhenius plot is commonly reported in the literature.[52,84] The activation energy for the ionic conductivity for Sm-, (Sm + Ca)- (Table 2), and In-doped samples (Table 3) was found to be lower than that of the parent $CeO_2$ and is comparable to that of doped $CeO_2$ reported in the literature.[99,100]

The oxygen self-diffusion coefficient ($D^*$) was determined for the $Ce_{0.9}Sm_{0.1}O_{1.95}$ sample using the Nernst−Einstein equation:

$$\sigma_i = \frac{4ne^2D^*}{k_BT} \quad (6)$$

where $\sigma_i$ is the ionic conductivity, $n$ is the number of oxide vacancies per unit volume, $k_B$ is Boltzmann's constant, $e$ is the electronic charge, and $T$ is the absolute temperature.[101−103] The diffusion coefficient was determined to be $2.08 \times 10^{-6}$ cm$^2$/s at 812 °C. Similar values were obtained for Sm-, (Sm + Ca)-, and In-doped cerates, which agrees with reported diffusion coefficients of similar cerium-doped materials ($Ce_{0.69}Gd_{0.31}O_{2-\delta}$, $D^* \approx 10^{-6}$ cm$^2$/s at 800 °C).[104]

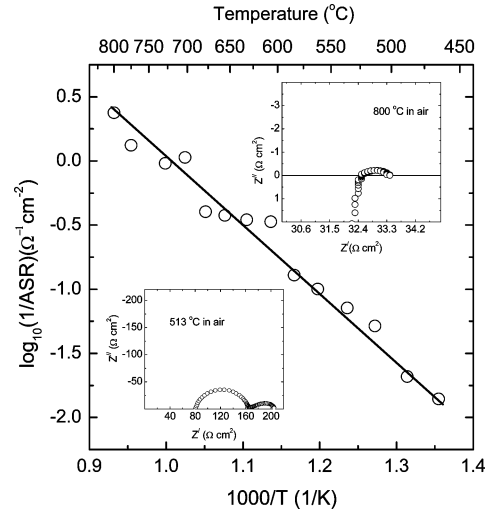


**Figure 14.** Plot of the area-specific polarization for the symmetric cell (Sm,Sr)$CoO_{3-x}$ (SSC)|$Ce_{0.8}Sm_{0.2}O_{1.9}$|(Sm,Sr)$CoO_{3-x}$. The line passing through the data set is a guide to the eye. The apparent activation energy was determined to be 1 eV. The corresponding impedance plots at 513 and 800 °C are shown as insets.

**3.3.3.. Characterization of $Ce_{0.8}Sm_{0.2}O_{1.9}$ with SSC Cathode.** Figure 14 shows the ASR plot for the symmetric cell composed of the $Ce_{0.8}Sm_{0.2}O_{1.9}$ electrolyte prepared via the ceramic method using an IT-SOFC cathode, Sr-doped $SmCoO_3$ (SSC). The SSC electrode was prepared in air via the ceramic method using corresponding metal salts and oxides at 1200 °C, and the PXRD pattern showed the formation of a single-phase perovskite structure (Figure 15b). The chemical reactivity of $Ce_{0.8}Sm_{0.2}O_{1.9}$ (Figure S7 in the Supporting Information) and $Ce_{0.8}Sm_{0.05}Ca_{0.15}O_{1.825}$ (Figure 15) with SSC was also conducted by mixing 1:1 weight ratios of the powders and sintering the mixture between 800 and 1200 °C. PXRD analysis shows the formation of a new phase at 1200 °C. The peaks at $2\theta \approx 36.7°$ and 42.6° could be due to the formation of CoO, which has a 100% peak at $2\theta \approx 42.4°$ and a 67% peak at $2\theta \approx 36.5°$ (JCPDS No. 48-1719), and $Co_3O_4$ also has a 100% peak at $2\theta \approx 36.8°$ (JCPDS Nos. 43-1003 and 42-1467). Accordingly, we have prepared the symmetric cell using a $Ce_{0.8}Sm_{0.2}O_{1.9}$ electrolyte and SSC electrodes at 1000 °C for ASR investigation. It was found that at high temperatures the impedance plot showed an overlap of the grain-boundary and electrode contributions (Figure 14, inset) and at low temperatures the appearance of the bulk, grain-boundary, and electrode semicircles is clearly visible. The apparent activation energy was deter-

(100) Faber, J.; Geoffroy, C.; Roux, A.; Sylvestre, A.; Abelard, P. *Appl. Phys. A: Mater. Sci. Process.* **1989**, *49*, 225–232.
(101) Raj, E. S.; Skinner, S. J.; Kilner, J. A. *Solid State Ionics* **2005**, *176*, 1097–1101.
(102) Kilner, J. A. *Solid State Ionics* **2000**, *129*, 13–23.
(103) Steele, B. C. H. *J. Power Sources* **1994**, *49*, 1–14.
(104) Ruiz-Trejo, E.; Sirman, J. D.; Baikov, Y. M.; Kilner, J. A. *Solid State Ionics* **1998**, *113−115*, 565–569.

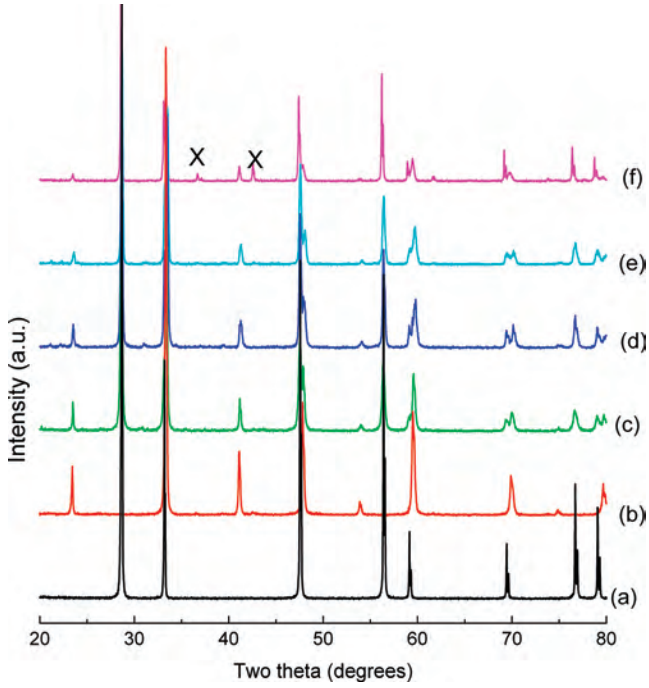


**Figure 15.** PXRD patterns showing the chemical stability of $Ce_{0.8}Sm_{0.05}Ca_{0.15}O_{1.825}$ with a SSC cathode up to 1200 °C. A 1:1 weight ratio of the materials was used: (a) $Ce_{0.8}Sm_{0.05}Ca_{0.15}O_{1.825}$ as prepared using $CO_2$ capture; (b) SSC prepared using the ceramic method; (c) 1:1 mixture of as-prepared powders; (d) mixture sintered at 900 °C; (e) mixture sintered at 1000 °C; (f) mixture sintered at 1200 °C for 24 h. New phases due to CoO and $Co_3O_4$ are marked with X in part f.

mined to be 1 eV, which is comparable to literature values.[105−108]

The electrochemical stability of $CO_2$ capture method synthesized $Ce_{0.8}Sm_{0.05}Ca_{0.15}O_{1.825}$with SSC electrodes over 5 days at 812 °C was also determined. It was found that the bulk resistance remains constant (Figure 16) and the grain-boundary and electrode contributions increased over the course of 1 week. The difference in the grain-boundary and electrode contributions over 5 days was approximately 2 Ω, indicating that the cerate is stable toward SSC electrodes at this temperature for 5 days.

## 4. Conclusions

Fast oxide-ion-conducting fluorite-type $Ce_{0.9}Sm_{0.1}O_{1.95}$, $Ce_{0.8}Sm_{0.2}O_{1.9}$, $Ce_{0.8}Sm_{0.05}Ca_{0.15}O_{1.825}$, $Ce_{0.9}In_{0.1}O_{1.95}$, and $Ce_{0.8}In_{0.2}O_{1.95}$ were successfully prepared from the corresponding barium perovskites after reaction with $CO_2$ at 800 °C. PXRD was used to understand the conversion of a perovskite into the fluorite structure, SEM was used to understand the morphology of the compounds, and ac impedance spectroscopy was used to investigate the materials

(105) Chang, A.; Skinner, S. J.; Kilner, J. A. *Solid State Ionics* **2006**, *177*, 2009–2011.
(106) Colomer, M. L.; Steele, B. C. H.; Kilner, J. A. *Solid State Ionics* **2002**, *147*, 41–48.
(107) Steele, B. C. H.; Bae, J. *Solid State Ionics* **1998**, *106*, 255–261.
(108) Hertz, J. L.; Tuller, H. L. *J. Electrochem. Soc.* **2007**, *154*, B413–B418.

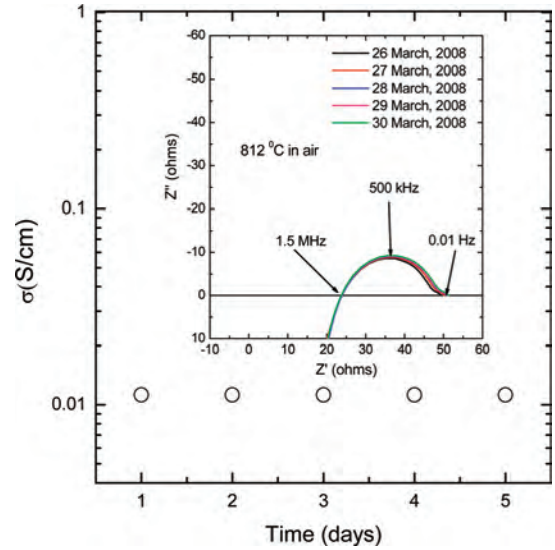


**Figure 16.** Electrical conductivity and ac impedance plots showing the stability of $Ce_{0.8}Sm_{0.05}Ca_{0.15}O_{1.825}$ with a SSC cathode over 5 days at 812 °C in air. The bulk resistance (high-frequency intercept) remains constant in the impedance plots, as shown in the inset.

ionic conductivity. It was found that the $CO_2$ capture per ceramic gram depends only on the barium content. The lattice constants and ionic conductivities of the Sm-doped samples are consistent with the literature. Our attempts to prepare $Ce_{0.9}In_{0.1}O_{1.95}$ and $Ce_{0.8}In_{0.2}O_{1.9}$ by the ceramic method at 800 and 1500 °C failed because PXRD showed the presence of both $CeO_2$ and $In_2O_3$. However, we successfully prepared single-phase In-doped $CeO_2$ using the $CO_2$ capture method. PXRD studies showed that In-doped $CeO_2$ materials prepared by $CO_2$ capture were thermodynamically unstable at temperatures above 800 °C, suggesting that the In-doped $CeO_2$ samples appear to be thermodynamically unstable at elevated temperatures. It must be mentioned that our attempts to prepare single-phase $Ce_{0.9}In_{0.1}O_{1.95}$ and $Ce_{0.8}In_{0.2}O_{1.9}$ via the ceramic method and sintering at 800 °C for 24 h yield PXRD patterns that consist of a biphasic material. Therefore, the $CO_2$ capture technique may be the only viable means to incorporate indium into a fluorite lattice.

**Acknowledgment.** We thank the Natural Sciences and Engineering Research Council (NSERC) of Canada and the Canada Foundation for Innovation (CFI) for financial support.

**Supporting Information Available:** Additional PXRD patterns showing the conversion of perovskite $BaCe_{0.9}Sm_{0.1}O_{2.95}$, $BaCe_{0.8}Sm_{0.2}O_{2.9}$, and $BaCe_{0.8}In_{0.2}O_{2.9}$ into fluorite $Ce_{0.9}Sm_{0.1}O_{1.95}$, $Ce_{0.8}Sm_{0.2}O_{1.9}$, and $Ce_{0.8}In_{0.2}O_{1.9}$, metastability of $Ce_{0.8}In_{0.2}O_{1.9}$ prepared by the $CO_2$ capture method, ac resisitvity of data, and chemical stability of $Ce_{0.8}Sm_{0.2}O_{1.9}$ with a Sr-doped $SmCoO_3$ (SSC) cathode up to 1200 °C. This material is available free of charge via the Internet at http://pubs.acs.org.

IC8010025